Published in final edited form as:
Arch Biochem Biophys. 2011 February 15; 506(2): 181–187. doi:10.1016/j.abb.2010.12.004.

Kinetic and Crystallographic Studies of the Role of Tyrosine 7 in the Active Site of Human Carbonic Anhydrase II

Rose Mikulski[a], **Balendu Sankara Avvaru**[b], **Chingkuang Tu**[a], **Nicolette Case**[a], **Robert McKenna**[*,b], and **David N. Silverman**[*,a]

[a]Department of Pharmacology, University of Florida, Gainesville, FL 32610, USA

[b]Department of Biochemistry and Molecular Biology, University of Florida, Gainesville, FL 32610, USA

Abstract

The rate limiting step in catalysis of bicarbonate dehydration by human carbonic anhydrase II (HCA II) is an intramolecular proton transfer from His64 to the zinc-bound hydroxide. We have examined the role of Tyr7 using site-specific mutagenesis and measuring catalysis by the ^{18}O exchange method using membrane inlet mass spectrometry. The side chain of Tyr7 in HCAII extends into the active-site cavity about 7 Å from the catalytic zinc atom. Replacement of Tyr7 with eight other amino acids had no effect on the interconversion of bicarbonate and CO_2, but in some cases caused enhancements in the rate constant of proton transfer by nearly 10-fold. The variant Y7I HCA II enhanced intramolecular proton transfer approximately two-fold; its structure was determined by X-ray crystallography at 1.5 Å resolution. No changes were observed in the ordered solvent structure in the active-site cavity or in the conformation of the side chain of the proton shuttle His64. However, the first eleven residues of the amino-terminal chain in Y7I HCA II assumed an alternate conformation compared with the wild type. Differential scanning calorimetry showed variants at position 7 had a melting temperature approximately 8 °C lower than that of the wild type.

Introduction

Carbonic anhydrases (CAs) are a family of predominantly zinc metalloenzymes found in nearly all forms of life. Carbonic anhydrase catalyzes the dehydration of bicarbonate and a proton into carbon dioxide and water by a two-stage mechanism (eqs 1, 2) [1–3] that appears to be a common feature in this diverse family of enzymes.

$$EZnH_2O+HCO_3^- \overset{-H_2O}{\rightleftharpoons} EZnHCO_3^- \rightleftharpoons EZnOH^-+CO_2 \quad (1)$$

*Corresponding authors: D.N.S. Department of Pharmacology, College of Medicine, University of Florida, Box 100267, Gainesville, Florida 32610; Phone: (352) 392 3556; Fax (352) 392 9696; silvrmn@ ufl.edu; R.M. Department of Biochemistry and Molecular Biology, College of Medicine, University of Florida, Box 100245, Gainesville, Florida 32610; Phone: 352-392-5696; Fax: 352-392-3422; rmckenna@ufl.edu.

SUPPLEMENTARY DATA

Supplementary data associated with this article can be found in the online version at ***

$$\text{His64} - \text{EZnOH}^- + \text{BH}^+ \rightleftharpoons \text{H}^+\text{His64} - \text{EZnOH}^- + \text{B} \rightleftharpoons \text{His64} - \text{EZnH}_2\text{O} + \text{B} \quad (2)$$

The first stage (eq 1) is the dehydration of bicarbonate by zinc-bound hydroxide and subsequent release of carbon dioxide leaving a hydroxide ion at the zinc. The second step in the dehydration direction (eq 2) requires proton transfer to zinc-bound hydroxide from bulk solvent. In many of the isozymes in the α class of CAs, including human carbonic anhydrase II (HCA II), His64 acts as a proton shuttle and provides a pathway for the transfer between bulk solvent and external buffer (B in eq 2). The side chain of His64 in HCA II lies on the rim of the active site cavity with two observed orientations in crystal structures: inward with the side chain pointing toward the zinc and outward with the side chain pointing towards bulk solvent [4, 5]. The intramolecular proton transfer in the second step (eq 2) is rate-limiting for the maximal velocity in well-buffered solutions [6,7]. Human carbonic anhydrase II promotes a highly rapid catalysis with a maximal turnover rate of about 1 μs^{-1}. For this reason, HCA II is a useful experimental and theoretical model to study the efficiency of proton transfers in a protein environment.

The active site cavity of HCA II has distinct hydrophilic and hydrophobic surfaces with the zinc ion at the bottom of a conical cavity. A chain of hydrogen bonded, ordered water molecules (W1, W2, W3a and W3b) extends from the zinc-bound water to the proton shuttle residue His64 [5] (Figure 1). The water network is maintained in part by interactions with hydrophilic residues within the active site cavity (Tyr7, Asn62, Asn67, Thr200). The significance of this ordered water network in rapid transfer of protons has been studied in various mutants of HCAII [8–14] as well as molecular dynamic simulations [15–18].

Among the residues of interest on the hydrophilic side of the active site cavity is Tyr7, which is a conserved residue in the mammalian as well as in many other isozymes of CA in the α class [19]. The side chain of Tyr7 in HCA II extends into the active site cavity with no apparent interactions with other residues (Figure 1). The hydroxyl of Tyr7 appears to be within hydrogen bonding distance of water molecule W3a. However, the neutron crystal structure recently determined at pH 9 shows the tyrosine hydroxyl unprotonated and no such hydrogen bond to solvent [9]. Initial studies by stopped-flow spectrophotometry using the mutant Y7F HCA II showed catalytic activity in hydration marginally reduced [10]. However, further examination using ^{18}O exchange showed that the proton transfer component of catalytic dehydration was enhanced as much as 9-fold compared to wild type [8].

Here we discuss a number of substitutions at position 7 in HCA II to provide further insight to the structural aspects influencing the rate of the intramolecular proton transfer step in the catalysis. Catalysis by each of the variants was studied by ^{18}O exchange between CO_2 and water using membrane inlet mass spectrometry, and the X-ray crystal structure of Y7I HCAII was determined at 1.5 Å resolution. We have found that substitution at Tyr7 had no effect on the first stage of catalysis (eq 1), but certain amino acids at position 7 showed enhanced rate constants for proton transfer, three-fold for Y7I and nearly 10-fold for Y7F compared with wild type. The variants with replacements at residue 7 had a lower thermal stability by about 8 °C and Y7I showed an altered conformation in the first eleven residues at the amino terminus. These studies emphasize the role of Tyr7 in establishing the fold of the N-terminus of HCA II and its influence in long range, intramolecular proton transfer.

Materials and Methods

Expression and purification of enzymes

Several variants of HCA II were created with the Stratagene Quick Change II site-directed mutagenesis kit (La Jolla, CA) on the expression vector coding the full-length wild type HCA II. Tyr 7 was replaced with Ala, Ile, Trp, Asp, Asn, Ser, and Arg. The DNA sequences of each single mutant were confirmed for the entire region coding of CA in the vector. The verified plasmids were then transformed for expression into *Escherichia coli* BL21(DE3)pLysS cells from Stratagene. The transformed cells were grown in LB media containing 1.0 mM $ZnSO_4$ and induced with IPTG to a final concentration of 1.0 mM at an OD_{600} of 0.6 AU [14]. Each variant of Try 7 was purified by affinity chromatography using p-(aminomethyl) benzenesulfonamide coupled to agarose beads (Sigma) [20]. Protein concentrations of variants were determined by titration with the tight-binding inhibitor ethoxolamide and detecting activity by ^{18}O exchange between CO_2 and water.

Kinetics—Catalysis was measured by the ^{18}O exchange method based on the measurement by membrane inlet mass spectrometry of the depletion of ^{18}O from species of CO_2 [21]. The apparatus uses a membrane probe of silastic tubing, which is permeable to dissolved gases and is submerged in the reaction solution. The probe is connected to glass tubing that runs through a dry-ice and acetone water trap and continues to the mass spectrometer (Extrel EXM-200) [22]. In the first of two independent stages of catalysis, the dehydration of labeled bicarbonate has a probability of transiently labeling the active site with ^{18}O (eq 3). In a second stage, the protonation of the zinc-bound, ^{18}O-labeled hydroxide results in the release of $H_2\,^{18}O$ to the solvent (eq 4).

$$HCOO^{18}O^- + EZnH_2O \rightleftharpoons EZnHCOO^{18}O^- \rightleftharpoons COO + EZn^{18}OH^- \quad (3)$$

$$H + His64 - Ezn^{18}OH^- \rightleftharpoons His64 - EZnH_2{}^{18}O \rightarrow His64 - EzbH_2O + H_2{}^{18}O \quad (4)$$

Two rates for the ^{18}O exchange catalyzed by CA are obtained by this method. The first is R_1, the rate of exchange of CO_2 and HCO_3^- at chemical equilibrium, as shown in eq 5. Here k_{cat}^{exch} is a rate constant for maximal interconversion of substrate and product, K_{eff}^{S} is an apparent binding constant for substrate to enzyme, and S indicates substrate, either CO_2 or bicarbonate. For the most accurate mechanisms K_{eff}^{S} will contain some terms related to the binding of both CO_2 and bicarbonate [23]. The ratio $k_{cat}^{exch}/K_{eff}^{CO2}$ is, in theory and in practice, equal to k_{cat}/K_m for hydration obtained by steady-state methods [23].

$$R_1/[E] = k_{cat}^{exch}[CO_2]/(K_{eff}^{CO2} + [CO_2]) \quad (5)$$

The second rate determined by this method is R_{H2O}, which is the rate of release ^{18}O labeled water from the active site (eq 4). RH2O is a measure that is dependent upon the donation of protons to the ^{18}O-labeled zinc-bound hydroxide. In eq 6, k_B is the rate constant for proton transfer to the zinc-bound hydroxide, and $(K_a)_{His64}$ and $(K_a)_{ZnH2O}$ are the ionization constants of the proton donor and zinc-bound water molecule.

$$R_{H2O}/[E] = k_B/([+(K_a)_{His64}/[H^+]][1+[H^+]/(K_a)_{ZnH2O}]) + R_{H2O}{}^0 \quad (6)$$

Here R_{H2O}^0 is a pH independent contribution introduced to provide a fit to data showing a plateau in k_B^{obs} at pH > 8. Fits of eqs 5 and 6 to the data were carried out using Enzfitter (Biosoft).

The rate constants k_B are presented in a free energy plot and fitted by the Marcus theory for proton transfer [24] as applied to catalysis by carbonic anhydrase as described in earlier work [25,26]. The observed activation barriers are obtained from the pH independent, maximal values k_B, as in $\Delta G^{\ddagger}_{obs} = -RT\ln(hk_B/kT)$, where h is the Planck constant and k is the Boltzmann constant. The observed free energy of reaction is obtained from ΔpK_a of the reactants, $\Delta G^o = RT\ln[(K_a)_{acceptor}/(K_a)_{donor}]$. In the Marcus approach, the observed overall activation energy for proton transfer $\Delta G^{\ddagger}_{obs}$ is described in terms of the standard free energy of reaction ΔG^o and an intrinsic kinetic barrier $\Delta G^{\ddagger}_o$. This approach is further modified to describe proton transfers in which there is a component of the observed activation barrier that does not depend on ΔG^o for the reaction. This component is called the work term w^r for the forward direction (dehydration here) and w^p for the reverse. The Marcus equation then becomes:

$$\Delta G^{\ddagger}_{obs} = w^r + (1 + [\Delta G^o_{obs} - w^r + w^p]/4\Delta G^{\ddagger}_o)^2 \Delta G^{\ddagger}_o \quad (7)$$

The catalyzed and uncatalyzed exchanges of ^{18}O between CO_2 and water at chemical equilibrium were measured in the absence of buffer at a total substrate concentration of 25 mM of all species of CO_2 using membrane-inlet mass spectrometry. The temperature was 25 °C and the total ionic strength of solution was kept at a minimum of 0.2 M by the addition of Na_2SO_4. The stability of these enzymes made it necessary to work with fresh samples and keep them on ice. The kinetics on HCA II Y7F were reported earlier [8].

The hydrolysis of 4-nitrophenylacetate uncatalyzed and catalyzed by variants of CA were measured by the method of Verpoorte et al. [27]. Initial velocities were measured using a Beckman Coulter DU 800 spectrophotometer. The pH profiles of k_{cat}/K_M were fit to a single ionization with a maximum at high pH using Enzfitter (Biosoft).

Differential scanning calorimetry (DSC)

DSC experiments were performed using a VP-DSC calorimeter (Microcal, Inc., North Hampton, MA) with a cell volume of ~0.5 ml. Variants of HCA II were buffered in 50 mM Tris-Cl, pH 8.0 at protein concentrations of 50 μM. DSC scans were collected from 30 to 90 °C with a scan rate of 60 °C/hr. The calorimetric enthalpies (ΔH °m) of unfolding were calculated by integrating the area under the peaks in the thermograms after adjusting the pre- and post-transition baselines. The thermograms were fit to a two state reversible unfolding model to obtain van't Hoff enthalpies (ΔH^{vH}) of unfolding [28].

Crystallization and X-ray data collection

Crystals of the Y7I HCA II mutant were obtained using the hanging drop method [29]. The crystallization drops were prepared by mixing 5 μL of protein (concentration ~10 mg/mL in 10 mM Tris-Cl (pH 8.0)) with 5 μL of the precipitant solution (1.7 M sodium citrate 100 mM Tris-Cl (pH 8.0)) against a well of 1 mL precipitant solution. A few crystals were observed approximately one month after the crystallization setup at 293 K.

The X-ray diffraction data collection of a Y7I HCA II crystal was obtained at room temperature using an R-AXIS IV^{++} image plate system with Osmic mirrors and a Rigaku HU-H3R Cu rotating anode operating at 50 kV and 100 mA. The detector-to-crystal distance

was set to 100 mm and data were collected using oscillation steps of 1° with a 7 minute exposure per image. The data were processed and scaled using HKL2000 [30].

The crystal structure of HCA II (PDB accession code: 2ILI) (5) was used to obtain initial phases for the structure determination using SHELX97 (28). The zinc and all solvent molecules were removed to avoid model bias. 5% of the unique reflections were selected randomly and excluded from the refinement data set for the purpose of R_{free} calculations (29). Structural refinement used SHELXL initially with data from 50.0 to 1.5 Å resolution. The protein geometry was defined using the default constrains of conjugate-least squares (CGLS) mode in SHELXL. Each round of CGLS comprised of 15 cycles of refinement. $2F_o–F_c$ and $F_o–F_c$ electron density Fourier difference maps were calculated after each successive round of CGLS and manually inspected by the graphics program COOT (30) for further fine-tuning of the model and the incorporation of solvent molecules.

RESULTS

Catalysis

The site-specific mutants of HCA II in Table 1 were investigated for their catalytic properties using membrane inlet mass spectrometry measuring the rate of exchange of ^{18}O between CO_2 and water. The efficiency of the catalyzed hydration of CO_2 was measured as the rate constant $k_{cat}^{exch}/K_{eff}^{CO2}$ (eq 5) over a pH range of 5.0 to 9.0. The pH profiles for $k_{cat}^{exch}/K_{eff}^{CO2}$ by the mutants under study were adequately fit to a single ionization and appeared similar to that of the wild type (Figure 2, Supplementary Data, Figures S1, S2). The resulting maximal values of $k_{cat}^{exch}/K_{eff}^{CO2}$ represent catalytic activity in the hydration direction and were essentially identical to that of wild type (Table 1). The variation was greater for the activities k_{cat}/K_m for the catalyzed hydrolysis of p-nitrophenylacetate (Table 1). This probably reflects the larger size of the substrate for the ester hydrolysis which is influenced more by amino acid changes at position 7. The resulting values of $pK_{a\ ZnH2O}$ representing the ionization of the zinc-bound water for each mutant are listed in Table 2. The data demonstrate that the values of pK_{aZnH2O} of the zinc-bound water are near 7 for wild type and mutants. These $pK_{a\ ZnH2O}$ values were determined both by measurement of esterase activity and ^{18}O exchange (Table 2).

The pH profiles of the rate constant $R_{H2O}/[E]$ (Figures 3, S3, S4) provide three constants relevant to the catalysis, according to eq 6. The first is an estimate of $pK_{a\ ZnH2O}$, values which are given in Table 2 and generally are consistent with the values described in the above paragraph. Exceptions are Y7A, Y7S, and Y7R (Table 2; Figures S3,S4). These differences may be due to different properties of the active site for the processes of eq 3 and eq 4, or possibly difficulty interpreting the irregular curves for RH2O during catalysis by Y7A and Y7S (Figures S3,S4). The pH profile for $R_{H2O}/[E]$ in catalysis by Y7D did not have sufficient bell shape to assign values of pK_a. In later construction of a free energy plot, we have used data only from R_{H2O}.

The second constant is a value of $pK_{a\ His64}$ (Table 2). These values are uniformly lower for replacements at residue 7 than the value of $pK_{a\ His64}$ at 7.2 in wild type HCA II (Table 2). Such a shift in $pK_{a\ His64}$ is associated with the inward coordination of the side chain of His 64 [8,14] and its more hydrophobic environment than in wild type HCA II in which this side chain appears about equally in inward and outward orientations [4,5]. The third constant is the maximal, pH-independent value of k_B describing intramolecular proton transfer in the dehydration direction obtained by a fit to eq 6 to the pH profiles for $R_{H2O}/[E]$ (Table 1; Figures 3, S3, S4). The pH profiles for R_{H2O}, from which k_B values were obtained, were more difficult to fit for Y7D and Y7N than the bell curve of wild type HCA II and other variants. The data for Y7I were consistent with a value of k_B of 2.3 μs^{-1} from a fit of Figure

3. The greatest change in k_B among these variants was found for Y7F with a value of 7 μs^{-1} (Table 1).

Structure of Y7I HCA II

Crystals of Y7I HCA II were well ordered and diffracted X-rays to 1.5 Å resolution. Refinement and final model statistics are given in Table 3. The structures of Y7I and Y7F HCA II are similar to wild type in that the residues coordinating the zinc and those in the active site cavity (with the exception of residue seven) are unchanged (Figures 1, 4). Moreover, both show His64 predominantly in the inward orientation (Figure 4). A least-squares superposition of the crystal structure of Y7I onto wild-type HCA II (PDB ID: 2ILI [5]) yielded an average RMSD of 0.30 Å. However, the structure of Y7I HCAII showed several interesting features not present in the structures of wild type or of Y7F HCA II reported earlier [8]. Most notably there was a novel conformation of residues 4 to 11 of the N-terminal chain (Figure 5); the amino-terminal residues 1–4 were not observed in the crystal structure presumably because of disorder. This N-terminal conformation in Y7I HCA II caused the side chain of Ile7 to point away from the metal in the active site; the side chain of Ile7 does not occupy a position analogous to the side chain of Tyr7 in wild type, which lies between Thr200 and His64 (Figure 4). Despite the differences in structure of the N-terminal residues of Y7I and wild type, the geometry of the residues coordinating the zinc and the active site solvent structures were not altered (Figures 1,4).

Thermal Stability

The thermal stability of HCA II mutants was determined by differential scanning calorimetry (DSC). A single peak representing the main unfolding transition was observed for all of the variants of Table 1 and is shown for wild type, Y7I and Y7F HCA II in Figure 6. The fit to these data was based on a two state, reversible unfolding model to obtain the thermodynamic parameters. The main unfolding transition of the wild-type enzyme T_m occurred at 59.5 ± 0.5 °C and that of Y7I occurred at 51.8 ± 0.5 °C. The values of T_m for each of the remaining variants of Table 1 were between 49.3 and 52.5 °C except Y7F which had a distinctly broad transition with a T_m of 55.8 ± 0.5 °C (Figure 6). The calorimeteric parameters determined from the DSC experiments and the calculated thermodynamic parameters for all the HCA II mutants examined are listed in Table S1.

DISCUSSION

A notable result of this study of variants at residue 7 of HCA II is that the rate constants $k_{cat}^{exch}/K_{eff}^{CO2}$ for the first stage of catalysis (eqs 1, 3; Table 1) are unchanged. The substitutions of Tyr7 in wild type did not affect the ability of the protein to carry out the first stage of the catalysis. This appears to be a result of the amino acid substitutions being at least 7Å away from the zinc where the interconversion between CO_2 and bicarbonate occurs. However, among the variants of Table 1, there is range of increases and no decreases in the rate constants k_B for proton transfer from His64 to the zinc-bound hydroxide in the dehydration direction. The neutron diffraction structure of HCA II at pH 9.0 shows residue 7 as a tyrosinate ion [9]; the appearance of such an ion apparently has little influence on proton transfer since it can be replaced with a nonionic residue (Y7A) with no effect. In addition, the replacement of residue 7 caused decreases in thermal stability by up to 8 °C, and the single replacement of Tyr7 with Ile caused a major alteration in the conformation of the N-terminal chain in the Y7I structure (Figure 5). The amino terminal 11 residues were displaced with respect to their conformation in wild type with the side chain of Ile7 pointing away from the active site, different than for Tyr7 in wild type. The rate constant for proton transfer for Y7I HCA II was enhanced nearly 3-fold compared with wild type (Table 1).

Despite the large changes in the N-terminal region of Y7I HCA II, the structure of its active site is remarkably similar to that of the wild type enzyme including the network of ordered water molecules (Figures 1, 4), unlike Y7F HCAII in which water molecule W3a is not observed. In the crystal lattice, Ile 7 of Y7I rests in one of the crystal contact regions. Its amide nitrogen forms a hydrogen bond with the carboxyl side chain of Glu 238 and its side chain is in hydrophobic contact with Leu 240 (Figure S5). These interacting amino-acids are located in a single crystal-contact patch. It is possible that the altered orientation of the N-terminus of Y7I HCA II is a consequence of crystal contacts. It is interesting to note however, that this mutant crystallizes in the same space group as the wild type enzyme. After repeated attempts to crystallize other mutants listed in Table 1, only Y7I and Y7F HCA II have been successful. It is possible that mutations at Try 7 produce a disordered (or alternate) N-terminal conformation giving rise to structural heterogeneity in the samples, which is likely to deter crystal growth. Truncation of as many as 24 residues of the N-terminal end of HCA II does not prevent the remaining protein from folding correctly, and the structure of the N-terminus has been shown to form very late in folding [31].

A comparison of the characteristics of Y7I and Y7F HCA II reveals that they both have His64 in the inward orientation, both have values of ΔpKa ($pK_{a\ ZnH2O} - pK_{a\ His64}$) near 1.0, and both have nearly identical values of $k_{cat}^{exch}/K_{eff}^{CO2}$. However, they differ in their values of k_B, the rate constant for proton transfer in the dehydration direction, as shown in Table 1. This difference is shown in a free energy plot based on *kB* in Figure 7. The open circles are rate constants for proton transfer during catalysis by H64A HCA II determined by enhancement of catalysis when proton donors are exogenous derivatives of imidazole and pyridine [13]. These data are fit by Marcus theory applied to proton transfer (eq 7)[26,32], represented by the solid line of Figure 7. We assume this line represents the dependence of k_B on ΔpK_a within the active site. The significance of this fit is that these values of k_B are for proton transfer from donors not attached to the enzyme through chemical bonds, free of many restraints. Interestingly, the values of k_B for wild type HCA II and nearly all of the variants of Table 1, except Y7F HCA II, fall on or near this Marcus line (Figure 7).

We suggest that the reason the value of k_B for Y7F lies considerably above the Marcus line of Figure 7 while Y7I and other mutants lie closer to the line is the abbreviated water structure of Y7F. A significant difference is that Y7F has an unbranched, hydrogen-bonded water structure in the active site cavity (Figures 1, 4) compared to the wild type and Y7I enzyme. In solution these water structures have a lifetime in the picosecond range; however, the ordered water in the crystal structures provides a clue to the more stable water structures in catalysis. Computational studies of the proton transfer step in catalysis by carbonic anhydrase show that water wires consisting of fewer molecules transfer protons more efficiently [33,34]. Wild-type HCA II and Y7I have an identical water structure in the active-site cavity with a branched cluster of four ordered water molecules between His64 and the zinc bound water (Figures 1,4). In contrast, Y7F has a smaller, unbranched cluster of three water molecules that is more stable and provides a proton transfer pathway of lower energy barrier than wild type [34]. This provides an explanation of why Y7I and wild type, as well as other mutants, lie on the line of Figure 7 but Y7F lies above it, other variables being equal.

It is interesting to speculate why Tyr7 is conserved when substitution can enhance the rate of maximal catalysis. Calorimetry showed that the replacements of Try7 in HCA II decreased the thermal stability of the protein by 7 – 10 °C, except for Y7F which was decreased about 4 °C (Table S1). This decrease indicates that Tyr 7 stabilizes the enzyme, although it is unclear how it does this since the side chain of Tyr 7 has no apparent interactions with other residues in the crystal structure. At any rate, this decreased stabilization may be a factor to explain the occurrence of Tyr7 in many of the carbonic anhydrases in the α class. Tyr7 also

promotes folding of the N-terminal chain, which appears to have another role. A conserved N-terminus is consistent with this region of HCA II binding to the Cl^-/bicarbonate anion exchange proteins (AE) [35]. Recent deletion and mutation studies have shown the numerous histidine residues (His3,His4, His10, His15 and His 17) found in the N-terminus of HCA II represent an acidic motif important for binding the C-terminus of AE1 and AE2 [35].

Supplementary Material

Refer to Web version on PubMed Central for supplementary material.

Acknowledgments

This work was supported by a grant from the National Institutes of Health (GM 25154).

REFERENCES

1. Christianson DW, Fierke CA. Carbonic anhydrase: Evolution of the zinc binding site by nature and by design. Accounts of Chemical Research. 1996; 29:331–339.
2. Lindskog S. Structure and mechanism of carbonic anhydrase. Pharmacol Ther. 1997; 74:1–20. [PubMed: 9336012]
3. Silverman DN, Lindskog S. The Catalytic Mechanism of Carbonic-Anhydrase - Implications of a Rate-Limiting Protolysis of Water. Accounts of Chemical Research. 1988; 21:30–36.
4. Nair SK, Christianson DW. Unexpected pH-Dependent Conformation of His-64, the Proton Shuttle of Carbonic Anhydrase-II. Journal of the American Chemical Society. 1991; 113:9455–9458.
5. Fisher SZ, Maupin CM, Budayova-Spano M, Govindasamy L, Tu C, Agbandje-McKenna M, Silverman DN, Voth GA, McKenna R. Atomic crystal and molecular dynamics simulation structures of human carbonic anhydrase II: Insights into the proton transfer mechanism. Biochemistry. 2007; 46:2930–2937. [PubMed: 17319692]
6. Tu CK, Silverman DN, Forsman C, Jonsson BH, Lindskog S. Role of histidine 64 in the catalytic mechanism of human carbonic anhydrase II studied with a site-specific mutant. Biochemistry. 1989; 28:7913–7918. [PubMed: 2514797]
7. Steiner H, Jonsson BH, Lindskog S. Catalytic Mechanism of Carbonic-Anhydrase - Hydrogen-Isotope Effects on Kinetic-Parameters of Human C Isoenzyme. European Journal of Biochemistry. 1975; 59:253–259. [PubMed: 1249]
8. Fisher SZ, Tu CK, Bhatt D, Govindasamy L, Agbandje-McKenna M, McKenna R, Silverman DN. Speeding up proton transfer in a fast enzyme: kinetic and crystallographic studies on the effect of hydrophobic amino acid substitution in the active site of human carbonic anhydrase II. Biochemistry. 2007; 42:3803–3813. [PubMed: 17330962]
9. Fisher SZ, Kovalevsky AY, Domsic JF, Mustyakimov M, McKenna R, Silverman DN, Langan PA. Neutron Structure of Human Carbonic Anhydrase II: Implications for Proton Transfer. Biochemistry. 2010; 49:415–421. [PubMed: 20025241]
10. Liang ZW, Xue YF, Behravan G, Jonsson BH, Lindskog S. Importance of the Conserved Active-Site Residues Tyr7, Glu106 and Thr199 for the Catalytic Function of Human Carbonic Anhydrase-Ii. European Journal of Biochemistry. 1993; 211:821–827. [PubMed: 8436138]
11. Jackman JE, Merz KM Jr, Fierke CA. Disruption of the active site solvent network in carbonic anhydrase II decreases the efficiency of proton transfer. Biochemistry. 1996; 35:16421–16428. [PubMed: 8987973]
12. Krebs JF, Ippolito JA, Christianson DW, Fierke CA. Structural and Functional Importance of a Conserved Hydrogen-Bond Network in Human Carbonic Anhydrase-Ii. Journal of Biological Chemistry. 1993; 268:27458–27466. [PubMed: 8262987]
13. An H, Tu C, Duda D, Montanez-Clemente I, Math K, Laipis PJ, McKenna R, Silverman DN. Chemical rescue in catalysis by human carbonic anhydrases II and III. Biochemistry. 2002; 41:3235–3242. [PubMed: 11863462]

14. Zheng JY, Avvaru BS, Tu C, McKenna R, Silverman DN. Role of Hydrophilic Residues in Proton Transfer during Catalysis by Human Carbonic Anhydrase II. Biochemistry. 2008; 47:12028–12036. [PubMed: 18942852]
15. Maupin CM, Voth GA. Proton transport in carbonic anhydrase: Insights from molecular simulation. Biochimica Et Biophysica Acta-Proteins and Proteomics. 2010; 1804:332–341.
16. Maupin CM, McKenna R, Silverman DN, Voth GA. Elucidation of the Proton Transport Mechanism in Human Carbonic Anhydrase II. Journal of the American Chemical Society. 2009; 13:7598–7608. [PubMed: 19438233]
17. Riccardi D, Konig P, Guo H, Cui Q. Proton transfer in carbonic anhydrase is controlled by electrostatics rather than the orientation of the acceptor. Biochemistry. 2008; 47:2369–2378. [PubMed: 18247480]
18. Braun-Sand S, Strajbl M, Warshel A. Studies of proton translocations in biological systems: simulating proton transport in carbonic anhydrase by EVB-based models. Biophys J. 2004; 87:2221–2239. [PubMed: 15454425]
19. Hewett-Emmett D, Tashian RE. Functional diversity, conservation, and convergence in the evolution of the alpha-, beta-, and gamma-carbonic anhydrase gene families. Molecular Phylogenetics and Evolution. 1996; 5:50–77. [PubMed: 8673298]
20. Khalifah RG, Strader DJ, Bryant SH, Gibson SM. C-13 Nuclear Magnetic-Resonance Probe of Active-Site Ionizations in Human Carbonic-Anhydrase B. Biochemistry. 1977; 16:2241–2247. [PubMed: 16641]
21. Silverman DN. Carbonic anhydrase: oxygen-18 exchange catalyzed by an enzyme with rate-contributing proton-transfer steps. Methods Enzymol. 1982; 87:732–752. [PubMed: 6294458]
22. Tu CK, Swenson ER, Silverman DN. Membrane inlet for mass spectrometric measurement of nitric oxide. Free Radical Biology and Medicine. 2007; 43:1453–1457. [PubMed: 17936190]
23. Simonsson I, Jonsson BH, Lindskog S. C-13 NMR study of carbon dioxide-bicarbonate exchange catalyzed by human carbonic anhydrase-C at chemical-equilibrium. European Journal of Biochemistry. 1979; 93:409–417. [PubMed: 34514]
24. Marcus RA. Theoretical Relations among Rate Constants Barriers and Bronsted Slopes of Chemical Reactions. Journal of Physical Chemistry. 1968; 72 891-&.
25. Silverman DN, Tu C, Chen X, Tanhauser SM, Kresge AJ, Laipis PJ. Rate-equilibria relationships in intramolecular proton transfer in human carbonic anhydrase III. Biochemistry. 1993; 32:10757–10762. [PubMed: 8399223]
26. Kresge AJ, Silverman DN. Application of Marcus rate theory to proton transfer in enzyme-catalyzed reactions. Methods in Enzymology. 1999; 308:276–297. [PubMed: 10507009]
27. Verpoorte JA, Mehta S, Edsall JT. Esterase Activities of Human Carbonic Anhydrases B and C. Journal of Biological Chemistry. 1967; 242:4221–4229. [PubMed: 4964830]
28. Bruylants G, Wouters J, Michaux C. Differential scanning calorimetry in life science: Thermodynamics, stability, molecular recognition and application in drug design. Current Medicinal Chemistry. 2005; 12:2011–2020. [PubMed: 16101501]
29. McPherson, A. Preparation and Analysis of Protein Crystals. New York: Wiley; 1982.
30. Otwinowski Z, Minor W. Processing of X-ray Diffraction Data Collected in Oscillation Mode. Methods Enzymol. 1997; 276:307–326.
31. Aronsson G, Martensson LG, Carlsson U, Jonsson BH. Folding and Stability of the N-Terminus of Human Carbonic-Anhydrase-Ii. Biochemistry. 1995; 34:2153–2162. [PubMed: 7857926]
32. Marcus RA. H and other transfers in enzymes and in solution: Theory and computations, a unified view. 2. Applications to experiment and computations. Journal of Physical Chemistry B. 2007; 111:6643–6654.
33. Cui Q, Karplus M. Is a "proton wire" concerted or stepwise? A model study of proton transfer in carbonic anhydrase. Journal of Physical Chemistry B. 2003; 107:1071–1078.
34. Maupin CM, Saunders MG, Thorpe IF, McKenna R, Silverman DN, Voth GA. Origins of enhanced proton transport in the Y7F mutant of human carbonic anhydrase II. Journal of the American Chemical Society. 2008; 130:11399–11408. [PubMed: 18671353]

35. Vince JW, Carlsson U, Reithmeier RAF. Localization of the Cl-/HCO3- anion exchanger binding site to the amino-terminal region of carbonic anhydrase II. Biochemistry. 2000; 39:13344–13349. [PubMed: 11063570]

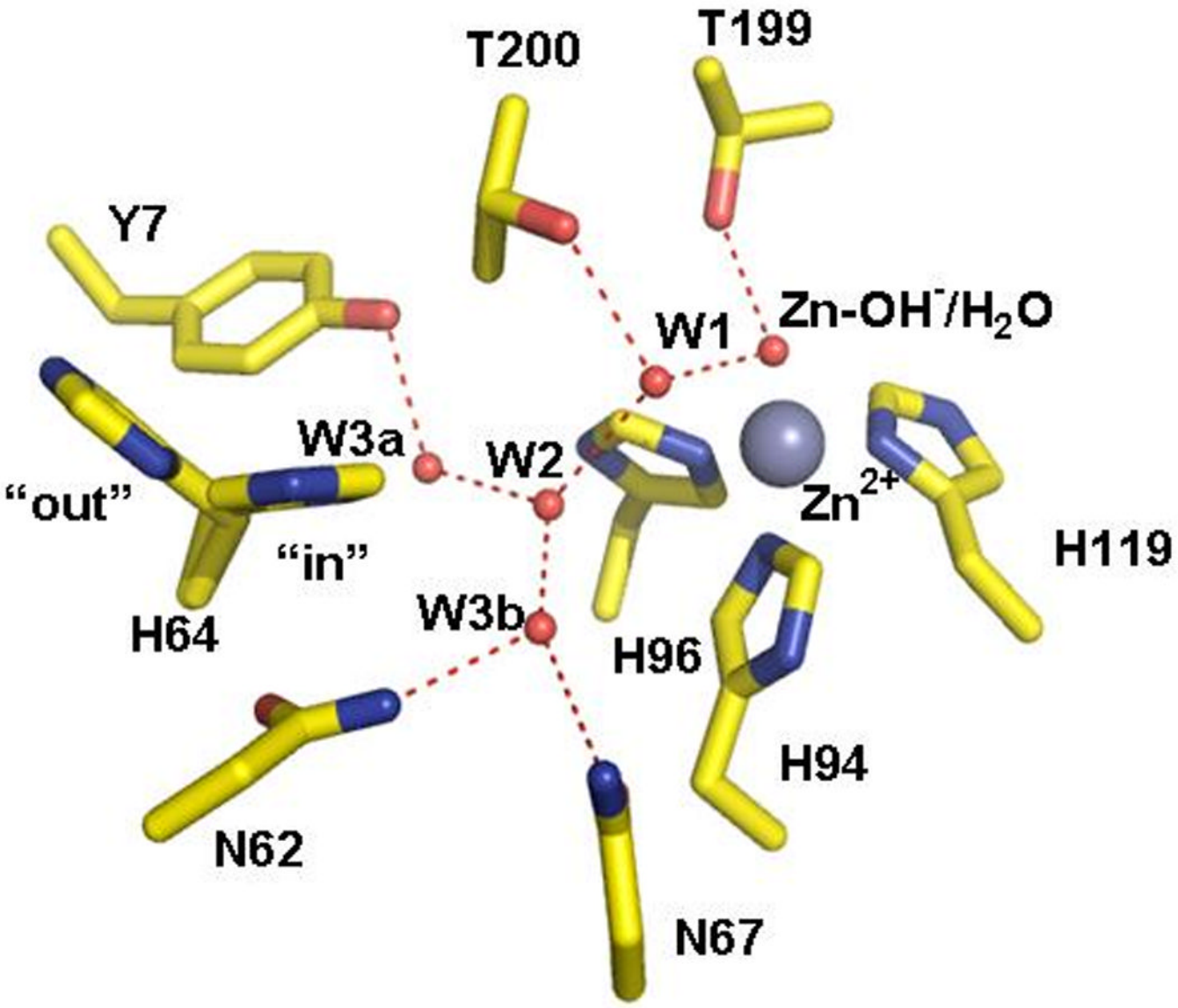

Figure 1.

Crystal structure of the active site region of wild type HCA II at 1.05 Å resolution and pH 7.8 from Fisher et al. (PDB ID 2ILI) [5] The zinc ion and the oxygen of water molecules are shown as gray and red spheres, respectively. The water network of the active-site is labeled W1, W2, etc. Dashed red lines are assumed hydrogen bonds. The side chain of the proton shuttle His64 is shown in both the inward and outward orientations. This figure was generated and rendered with PyMOL (www.pymol.org).

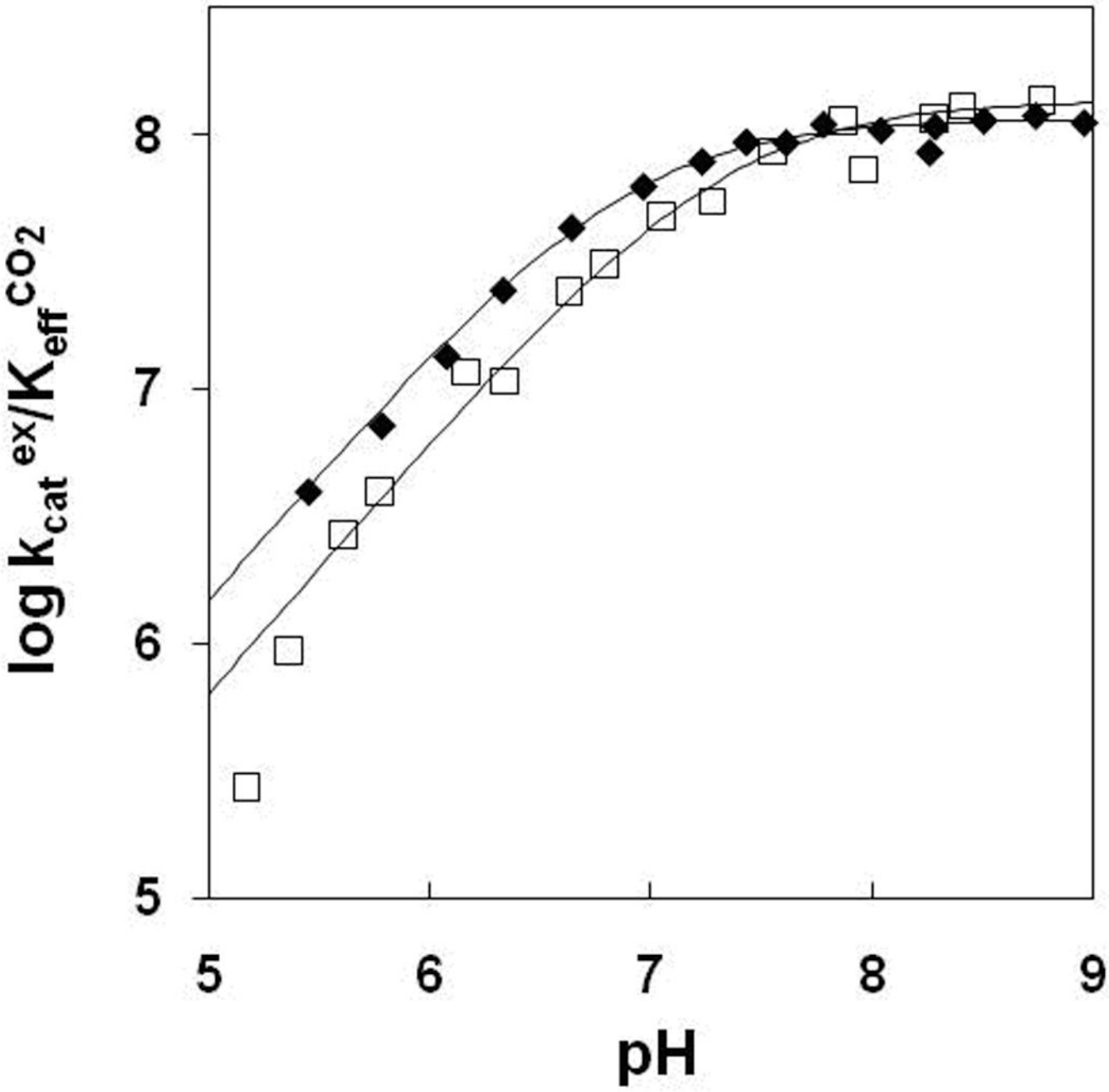

Figure 2.

The pH profiles for $k_{cat}^{ex}/K_{eff}^{CO2}$ ($M^{-1}s^{-1}$) for the hydration of CO_2 catalyzed by ( ) wild-type HCA II; and (□) Y7I HCA II. Data were obtained by ^{18}O exchange between CO_2 and water using solutions at 25 °C containing 25 mM of all species of CO_2 and sufficient Na_2SO_4 to maintain 0.2 M ionic strength.

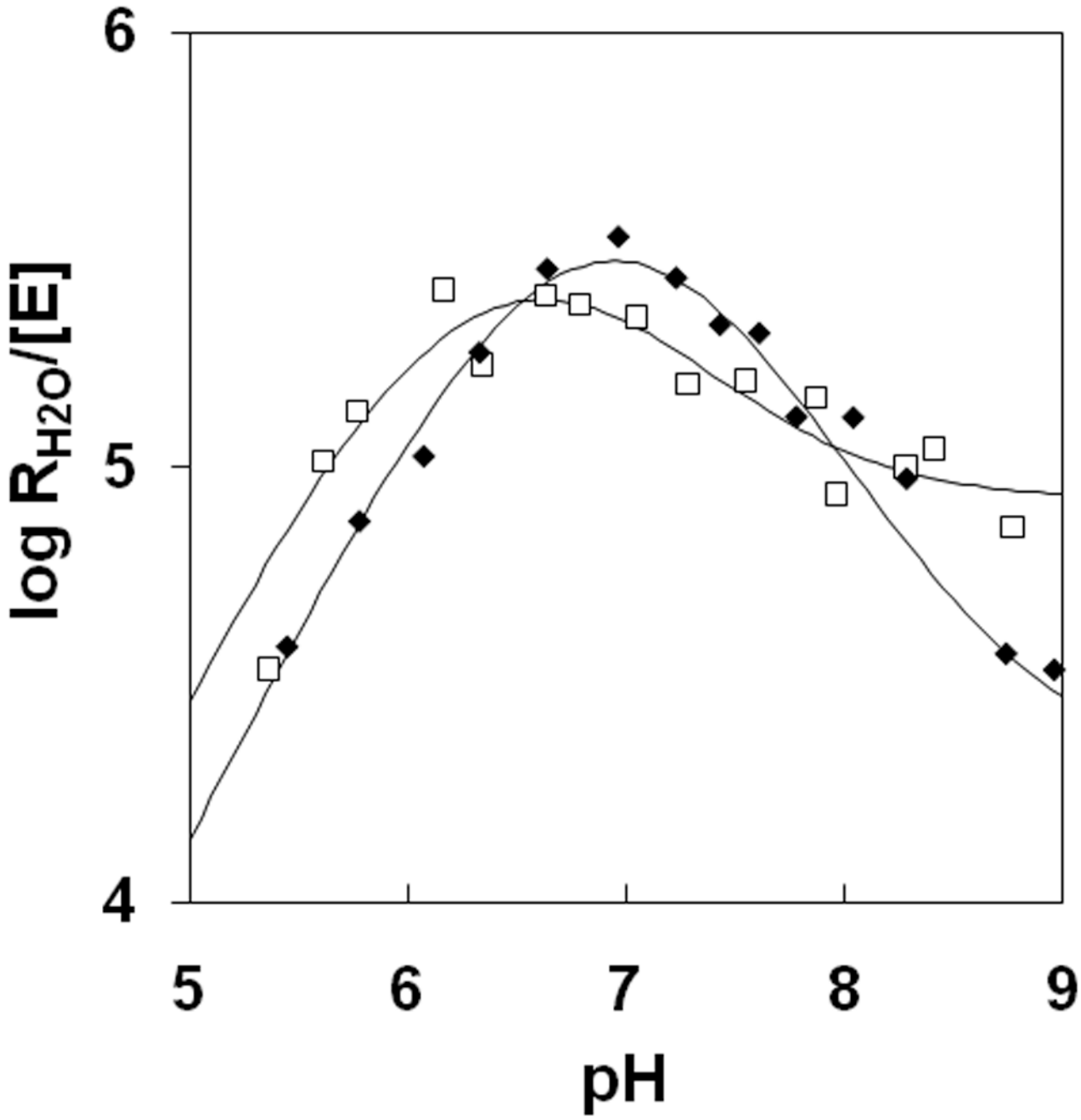

Figure 3.
The pH profiles for R_{H2O}/[E] (s^{-1}) the proton-transfer dependent rate of release of ^{18}O-labeled water catalyzed ( ) wild-type HCA II; and (□) Y7I HCA II. Conditions were as described in Figure 2.

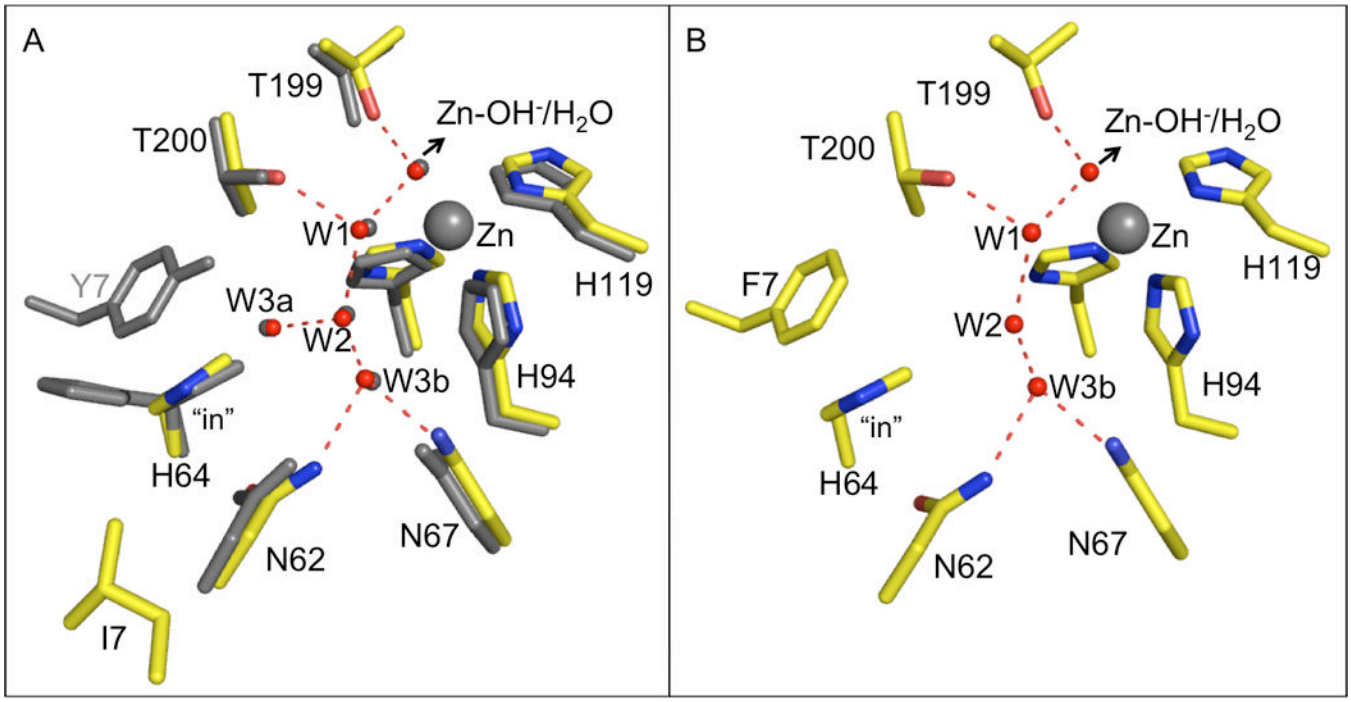

Figure 4.

Crystal structures of the active sites of (*A*) Y7I HCA II superimposed on wild-type HCA II which is shown in gray; and (*B*) Y7F HCA II from Fisher et al. [8]

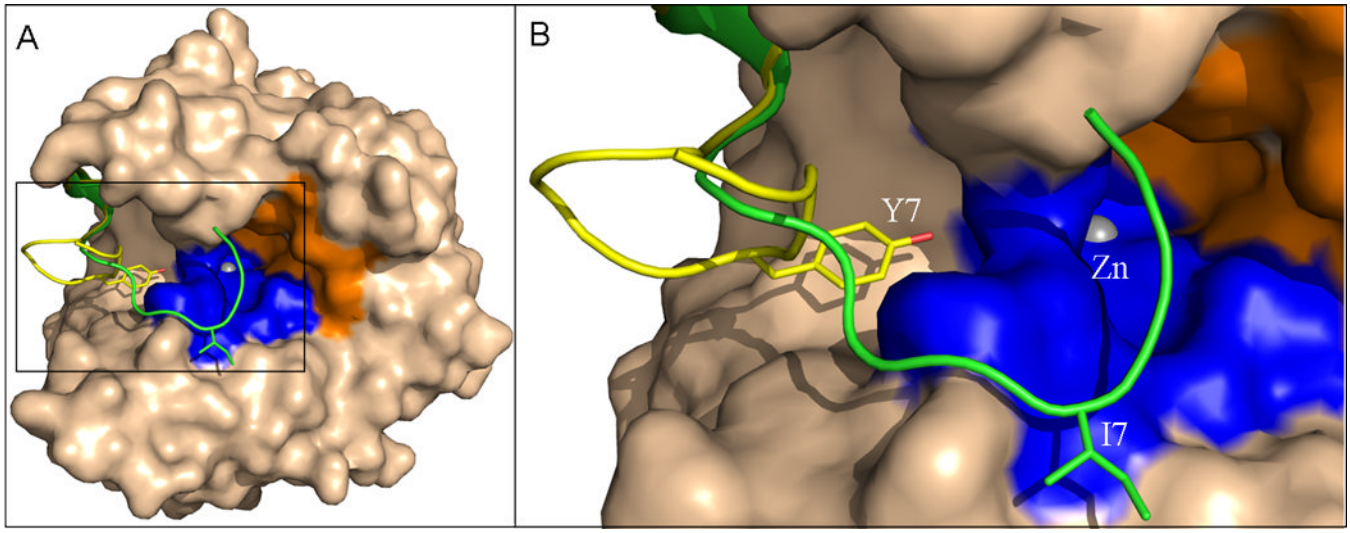

Figure 5.

Overall (A) and N-terminus (B) of superimposed crystal structures of wild-type HCA II and Y7I HCA II. The superimposed enzyme except the N-terminus is represented as a surface. The N-terminus of *(yellow)* wild type; and *(green)* Y7I HCA II is represented as ribbon, while the respective amino acids at position 7 as sticks. The hydrophobic and hydrophilic regions of the active-site are rendered orange and blue respectively. The active site zinc is depicted as a gray sphere.

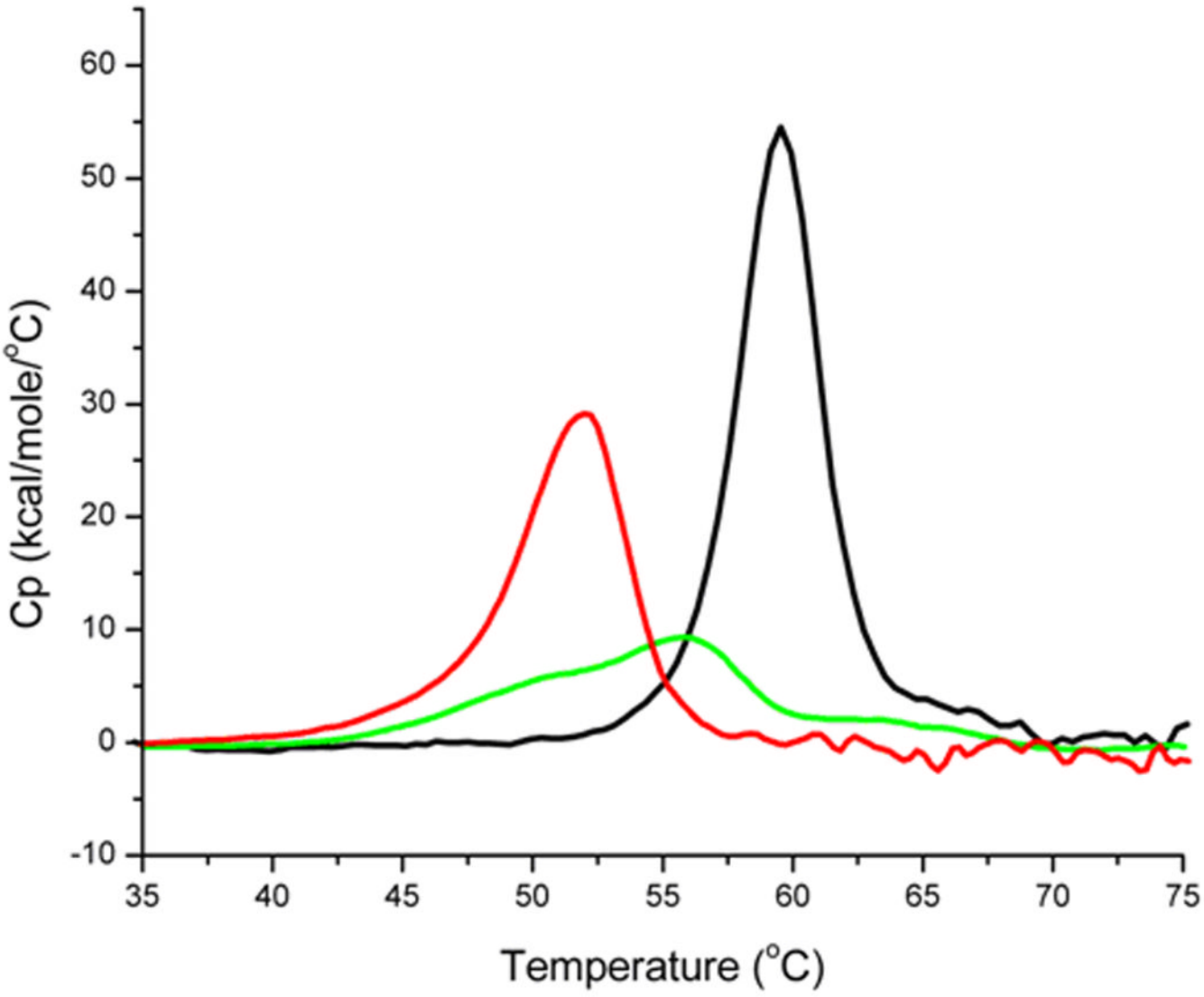

Figure 6.
Differential scanning calorimetry profiles of apparent excess specific heat (*Cp*) vs temperature for (*red*) Y7I HCA II; *(green)* Y7F HCA II and (*black*) wild-type HCA II.

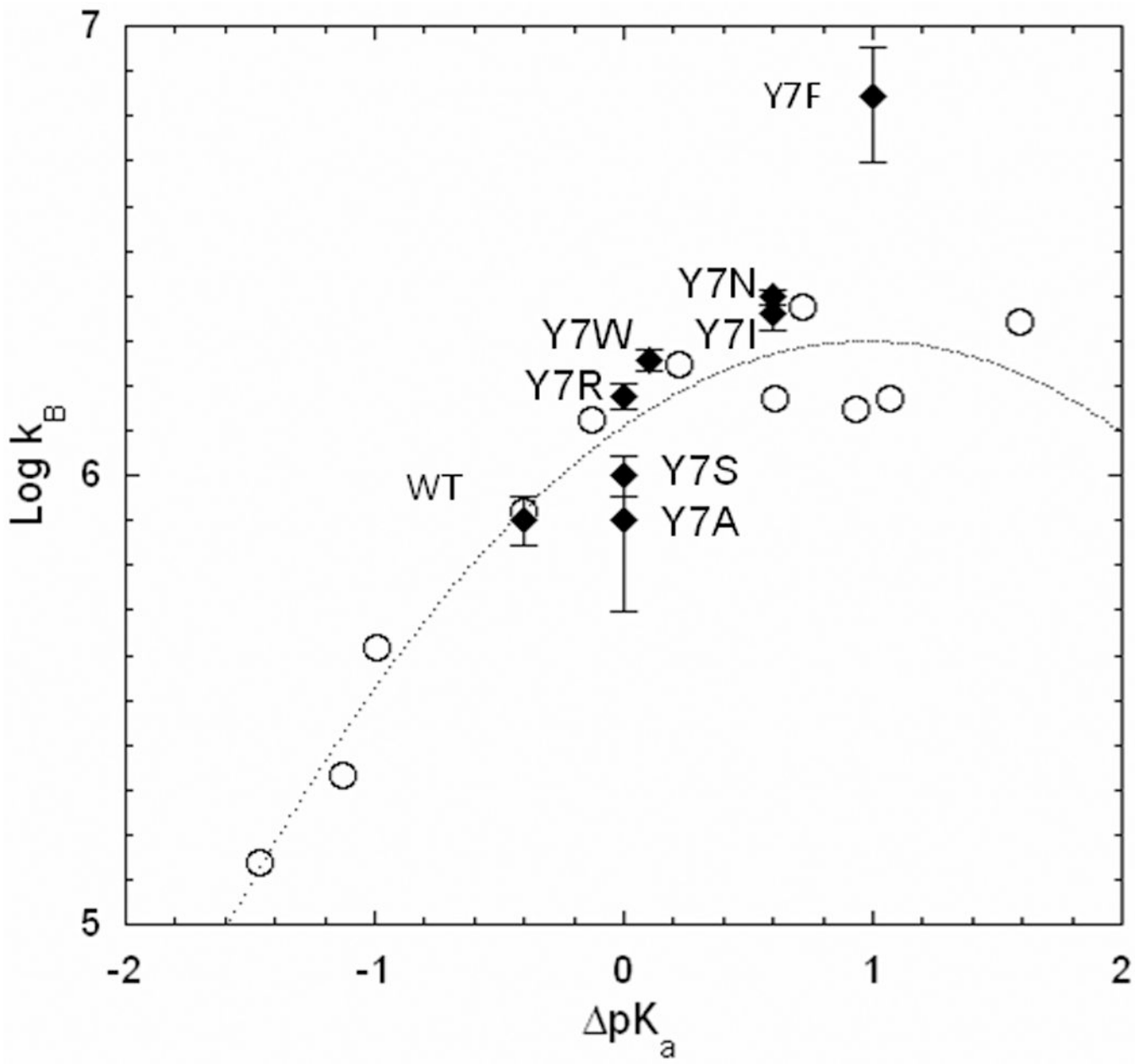

Figure 7.

Free energy plot of the logarithm of the rate constant for proton transfer k_B (s^{-1}) versus ΔpKa ($pK_{a\ ZnH2O} - pK_{a\ His64}$) determined from the R_{H2O}/[E] pH profiles for the wild type and the mutants of HCA II containing replacements of Tyr 7 identified on the plot (♦ *filled symbols*); and (○) for H64A HCA II from An et al. [13] with proton transfer provided predominantly by derivatives of imidazole and pyridine acting as exogenous proton donors with the solid line a best fit of Marcus Rate Theory.

Table 1

Maximal Values of Rate Constants for Hydration of CO_2, Hydrolysis of 4-Nitrophenylacetate, and Proton Transfer in Dehydration Catalyzed by HCA II and Variants.[a]

Enzyme	$k_{cat}^{exch}/K_{eff}^{CO2}$ CO_2 hydration ($\mu M^{-1}s^{-1}$) [b]	k_{cat}/K_m esterase ($M^{-1}s^{-1}$) [c]	k_B proton transfer (μs^{-1}) [d]
wild type	120	2800	0.8 ± 0.1
Y7I	130	2400	2.3 ± 0.2
Y7A	140	2300	0.8 ± 0.3
Y7W	140	1700	1.8 ± 0.1
Y7F [e]	120	4400	7 ± 0.2
Y7D	130	1800	0.8 ± 0.1 [f]
Y7N	100	1200	2.5 ± 0.1 [f]
Y7R	120	1700	1.5 ± 0.1
Y7S	100	1600	1.0 ± 0.1

[a] Derived from the kinetic curves for each substitution by a fit of to the data of Figures 2,3 and Supporting Information Figures S1–S4. All data were obtained at 25°C.

[b] Measured from the exchange of ^{18}O between CO_2 and water using eq 5 in the hydration direction. Standard errors here were less than 10%.

[c] Measured from the fit of the rate constants for ester hydrolysis to a single ionization. Standard errors here were less than 10%.

[d] Measured from the exchange of ^{18}O between CO_2 and water using eq 6 in the dehydration direction.

[e] Data are from Fisher et al. [8].

[f] These are maximal values of $R_{H2O}/[E]$ since incomplete pH profiles (Figures S3, S4) did not allow an adequate determination of k_B by a fit of eq 6.

Table 2

Values of Apparent pK_a Obtained by Various Kinetic Measurements of Catalysis by HCA II and Mutants

Enzyme	p$K_{a\ His64}$[a] (eq 6)	p$K_{a\ ZnH2O}$[a] (eq 6)	p$K_{a\ ZnH2O}$[b] (from $k_{cat}^{exch}/K_{eff}^{CO2}$)	p$K_{a\ ZnH2O}$ (esterase)
wild type	7.2 ± 0.1	6.8 ± 0.1	6.9 ± 0.1	6.9 ± 0.1
Y7I	6.2 ± 0.1	6.8 ± 0.1	7.1 ± 0.1	6.9 ± 0.1
Y7A	6.4 ± 0.2	6.4 ± 0.3	7.0 ± 0.1	7.2 ± 0.1
Y7W	6.9 ± 0.2	7.0 ± 0.3	7.2 ± 0.1	7.0 ± 0.1
Y7F [c]	6.0 ± 0.2[c]	7.0 ± 0.2[c]	7.1 ± 0.3[c]	7.0 ± 0.1
Y7D	-- [d]	-- [d]	6.4 ± 0.1	6.6 ± 0.2
Y7N	5.8 ± 0.1	6.4 ± 0.1	6.8 ± 0.1	6.4 ± 0.1
Y7R	6.2 ± 0.1	6.2 ± 0.1	7.4 ± 0.1	7.1 ± 0.1
Y7S	6.4 ± 0.1	6.4 ± 0.3	7.0 ± 0.1	6.9 ± 0.1

[a] Measured from the fits of eq 6.

[b] Measured from a fit of eq 5. As evident in these Figures, small perturbations were observed that could be fit by including a second ionization; however, these were not included in this Table.

[c] These data from Fisher et al. [8].

[d] For Y7D the data for R_{H2O}/[E] did not have sufficient bell-shape to be adequately fit by eq 6 (Figure S4).

Table 3

Crystal Structure Data and Refinement Statistics for Y7I HCA II

Data-collection statistics	
Temperature (K)	100
Wavelength (Å)	0.9724
Space group	P 2_1
Unit-cell parameters (Å,°)	a = 42.8, b = 41.6, c = 73.2, β =104.9
Total number of reflections Total number of unique reflections	507927 (43272)* 38859 (3606) *
Resolution (Å) $^a R_{sym}$ I/σ(I)	20.0-1.5 (1.55-1.5) * 9.9 (41.7) * 23.4 (3.5) *
$^b R_{cryst}$(%) $^c R_{free}$(%)	16.6 21.1
Amino acide residues	4–261
No. of protein atoms	2059
No. of H_2O molecules	186
R.m.s.d. for bond lengths (Å), angles (°)	0.007, 1.1
Ramachandran statistics (%) Most favored, additionally allowed and generously allowed regions	88.4, 11.1, 0.5
Average B factors (Å^2) main-, side-chain, Zn, solvent	17.3, 22.7, 11.7, 30.2

$^a R_{sym} = \Sigma |I - \langle I \rangle| / \Sigma \langle I \rangle$.

$^b R_{cryst} = (\Sigma ||Fo| - |Fc|| / \Sigma |F_{obs}|) \times 100$.

$^c R_{free}$ is calculated in same manner as $^b R_{cryst}$, except that it uses 5% of the reflection data omitted from refinement.

*Values in parenthesis represent highest resolution bin.